Physics Letters B 811 (2020) 135959

Contents lists available at ScienceDirect

Physics Letters B

www.elsevier.com/locate/physletb

Determining $B(E1)$ distributions of weakly bound nuclei from breakup cross sections using Continuum Discretized Coupled Channels calculations. Application to ^{11}Be

A.M. Moro [a,b,*], J.A. Lay [a,b], J. Gómez Camacho [a,c]

[a] Departamento de Física Atómica, Molecular y Nuclear, Facultad de Física, Universidad de Sevilla, Apartado 1065, E-41080 Sevilla, Spain
[b] Instituto Interuniversitario Carlos I de Física Teórica y Computacional (iC1), Apdo. 1065, E-41080 Sevilla, Spain
[c] Centro Nacional de Aceleradores, U. Sevilla, J. Andalucía, CSIC, Avda Thomas A Edison, 7, E-41092 Sevilla, Spain

ARTICLE INFO

Article history:
Received 27 April 2020
Received in revised form 16 November 2020
Accepted 16 November 2020
Available online 19 November 2020
Editor: J.-P. Blaizot

Keywords:
One-neutron halo nuclei
$dB(E1)/dE$
Coulomb breakup
Nuclear breakup
Coupled-channels methods

ABSTRACT

A novel method to extract the $B(E1)$ strength of a weakly bound nucleus from experimental Coulomb dissociation data is proposed. The method makes use of continuum discretized coupled channels (CDCC) calculations, in which both nuclear and Coulomb forces are taken into account to all orders. This is a crucial advantage with respect to the standard procedure based on the Equivalent Photon Method (EPM) which does not properly take into account nuclear distortion, higher order coupling effects, or Coulomb-nuclear interference terms. The systematic and statistical uncertainties of this procedure are evaluated. The procedure is applied to the ^{11}Be nucleus using two sets of available experimental data at different energies, for which seemingly incompatible $B(E1)$ have been reported using the EPM. We show that the present procedure gives consistent $B(E1)$ strengths, thus solving the aforementioned long-standing discrepancy between the two measurements.

1. Introduction

The investigation of nuclei close to the neutron and proton driplines require measuring observables which display their unusual structure properties. A relevant question is how the electromagnetic field connects the ground state of a weakly bound nucleus to its continuum. For that, one would ideally like to place the system under the action of a pure electromagnetic pulse, and observe the energy distribution of its fragments. In practice, this can be achieved experimentally by means of nuclear collisions, although these are sensitive not only to the Coulomb interaction but also to the nuclear interaction. By a suitable choice of the target, and an adequate range of scattering angles and collision energies, one can reduce the effect of the nuclear interaction, and have a Coulomb-dominated breakup reaction. Furthermore, under appropriate kinematical conditions, one can assume a simplified, first-order description of the reaction mechanism which leads to a proportionality of the observed experimental quantity, the breakup cross section distribution, with the structure property to be determined, which is the electric dipole $B(E1)$ distribution. This is the Equivalent Photon Method (EPM), for which the double differential breakup cross section, as a function of the scattering angle θ and the breakup energy ε is given by

$$\frac{d^2\sigma}{d\Omega d\varepsilon} = \frac{dB(E1,\varepsilon)}{d\varepsilon} F_1(\theta,\xi), \tag{1}$$

where $F_1(\theta,\xi)$ is the dipole Coulomb excitation function, which depends on the scattering angle and on the Coulomb adiabaticity parameter ξ, which is proportional to the excitation energy. This function was derived in the seminal work of Coulomb excitation of Alder and Winther [1]. At high energies, relativistic effects must be taken into account. This can be done using the generalization of Bertulani and Baur [2], in which the Coulomb excitation function is replaced by the number of virtual photons produced by the target $N_{E1}(\theta,\xi)$. They are related as:

$$F_1(\theta,\xi) = \frac{16\pi^3}{9\hbar c}\frac{dN_{E1}(\theta,\xi)}{d\Omega}. \tag{2}$$

Practical application of a Coulomb dissociation experiment involves considering a certain experimental angular range, determined by the experimental setup, over which the double differential cross section is integrated. Also, the measurements are performed at certain nominal breakup energies ε_i, which incorporate

* Corresponding author at: Departamento de Física Atómica, Molecular y Nuclear, Facultad de Física, Universidad de Sevilla, Apartado 1065, E-41080 Sevilla, Spain.
E-mail address: moro@us.es (A.M. Moro).

https://doi.org/10.1016/j.physletb.2020.135959

a distribution of nearby energies. Thus, the measured quantities are a discrete set of averaged differential cross sections σ_i, which, within the EPM approach, are given by

$$\sigma_i = \overline{B}(E1,\varepsilon_i)\overline{F}_1(\varepsilon_i), \tag{3}$$

where $\overline{F}_1(\varepsilon_i)$ is the dipole Coulomb function integrated over the angular and excitation energy ranges. Note that the value $\overline{B}(E1,\varepsilon_i)$ extracted from Eq. (3) should be understood as an average of the $B(E1)$ distribution over the energy range represented by ε_i, with weights determined by the integral of $F_1(\theta,\xi)$ over the angular range. This fact complicates the comparison of $\overline{B}(E1,\varepsilon_i)$ values obtained from different experiments, as well as these with theoretical calculations.

There are many approximations implicit in expressions (1) and (3). First, the semiclassical treatment should be valid, so that the scattering angle defines uniquely a classical trajectory, which is assumed to provide an accurate description of the quantum mechanical wave function. Second, the trajectories should be pure Coulomb, and should not be affected by the ever-present nuclear interaction. Third, the coupling interactions should be purely dipole Coulomb (no nuclear coupling), and have the asymptotic r^{-2} dependence over all the relevant range. Fourth, a first-order perturbation treatment of the Coulomb dipole force should be valid. Fifth, the effect of higher multipoles on breakup cross sections should be neglected. Moreover, the application of the integrated expression (3) requires that the aforementioned approximations should be valid for all the scattering angles contained in the experimental angular range.

In actual experiments, it can be argued that the EPM approximation is "fairly good", assuming that heavy targets are used, small angles are measured and the collision energy is adequate. This regime is optimistically referred to as "safe Coulomb" (see, e.g., Refs. [3,4]). However, even in these "safe Coulomb" cases, the EPM may have non-negligible deviations from more accurate calculations [5–7], which would go as uncontrolled systematic uncertainties to the $B(E1)$ distributions obtained from the breakup cross section using Eq. (3). Nuclear effects are sometimes taken into account by expressing the breakup cross sections σ_i^e as a sum of a nuclear contribution σ_i^n and a pure dipole Coulomb contribution,

$$\sigma_i^e = \sigma_i^n + \bar{B}(E1,\varepsilon_i)\bar{F}_1(\varepsilon_i). \tag{4}$$

The former is obtained experimentally re-scaling cross sections on nuclear-dominated reactions [8]. This procedure, however, neglects Coulomb-nuclear interference terms, as well as dynamical effects which may be very different in Coulomb and nuclear dominated reactions.

Taking into account the enormous efforts devoted to perform such experiments, aimed at getting $B(E1)$ distributions with the highest possible accuracy, it is timely to overcome the limitations of the EPM method and, whenever the approximations stated above are not well justified, substitute it by more accurate procedures based on the best quantum mechanical calculations available for the breakup cross sections. Several authors have already emphasized and quantified the importance of higher order effects in the analysis of Coulomb breakup experiments using a variety of methods, including semiclassical [9], quantum-mechanical [10,11], and dynamical eikonal [12,13] approaches (see also [14] for a review). With the same spirit, in this work we propose a new procedure to extract the $B(E1)$ distribution from Coulomb dissociation experiments, which relies on the Continuum-Discretized Coupled Channels (CDCC) method. CDCC is a well established fully quantum-mechanical reaction framework which does not require the approximations inherent to the EPM and overcomes most of its limitations. The procedure is applied to shed light on the apparently inconsistent $B(E1)$ distributions of ^{11}Be extracted from two different Coulomb dissociation experiments [8,15].

2. Theoretical procedure

The central idea of the present work is to provide a new methodology for determining $B(E1)$ distribution of halo nuclei from Coulomb dissociation experiments. The proposed method seeks a relation between the breakup cross sections and the underlying $B(E1)$ distribution which overcomes the aforementioned limitations of the EPM method. To find such a relation, the following strategy is adopted: We start with a structure model of the weakly bound nucleus. This model has to be as realistic as possible, but also sufficiently amenable to be used as an input for a full quantum mechanical scattering calculation for the reaction process. Next, reaction calculations are performed using this structure model as input. For that, in this work we adopt the Continuum-Discretized Coupled-Channels (CDCC) method which provides an approximate solution of the scattering problem in a truncated model space which includes the bound states of the weakly bound projectile and a discrete representation of the continuum states. In particular, we employ the extended CDCC (XCDCC) method [16,17] which, in addition to the halo degree of freedom, accounts for the core deformation and excitation. The projectile structure is described using a particle-plus-core model, comprising a core and one or two valence particles, with the core being described by a small number of discrete states. The model provides wavefunctions for the projectile bound and continuum states, from which a $B(E1)$ distribution, $dB^0(E1,\varepsilon)/d\varepsilon$, can be derived, which should be regarded only as an initial estimate of the $B(E1)$ distribution to be extracted from experiment. For the reaction calculations, the exact scattering states are replaced by a discrete representation, obtained by diagonalizing the projectile Hamiltonian in a truncated basis of square-integrable functions. In the calculations below, we adopt the Transformed Harmonic Oscillator (THO) basis employed in our previous works (e.g. Refs. [18,19]). The calculation, suitably integrated over the experimental setup, and including the angular and energy resolution, produces model differential cross sections σ_i^0, evaluated at the experimental energies ε_i. The model cross sections can be compared with the experimentally measured cross sections σ_i^e. The results will not coincide in general, as it should be expected from the fact that the model $B(E1)$ distribution does not coincide with the actual $B(E1)$ distribution of the projectile. However, we can use the model as a tool to investigate the relation between the $B(E1)$ distribution and the breakup cross section, which will be much more accurate than the EPM relation, Eq. (3), because it incorporates elements (quantum effects, nuclear forces, higher order coupling, etc) which are absent in the EPM.

As shown in the Appendix A, we can introduce small changes in the model, by multiplying all Coulomb dipole matrix elements by arbitrary factors $(1+\delta(\varepsilon_i))$ close to one. This modifies the $B(E1)$ distribution at each measured energy e_i,

$$B^m(E1,\varepsilon_i) \simeq B^0(E1,\varepsilon_i)(1+2\delta(\varepsilon_i)), \tag{5}$$

where $\delta(\varepsilon_i)$ is an energy dependent factor defined in Eq. (A.7). The differential cross sections will be also modified by the introduction of these renormalized dipole Coulomb couplings, in a non-trivial way, because the XCDCC calculations take into account couplings, nuclear and Coulomb, dipole and other multipoles, to all orders. However, a remarkable result, Eq. (A.11), is that the changes in the cross sections are determined by the same quantities $\delta(e_i)$, and a magnitude σ'_i, which is the derivative of the calculated cross sections with respect to $\delta(\varepsilon_i)$, and can be obtained from the model calculations as:

$$\sigma_i^m \simeq \sigma_i^0 + \delta(\varepsilon_i)\,\sigma'_i. \quad (6)$$

From Eqs. (5) and (6), one can eliminate the explicit dependence in $\delta(\varepsilon_i)$, leading to a relation between the $B(E1)$ distribution and the cross sections in the modified model:

$$B^m(E1,\varepsilon_i) \simeq B^0(E1,\varepsilon_i)\left(1+2\frac{\sigma_i^m-\sigma_i^0}{\sigma'_i}\right). \quad (7)$$

This gives an approximate linear relationship between $B^m(E1,\varepsilon_i)$ and σ_i^m.

The quantity σ'_i is the key magnitude that encodes the relation of cross sections and $B(E1)$ values. It plays the role of the dipole excitation function $\bar{F}(\varepsilon_i)$ in the EPM, and can be obtained from model calculations following Eq. (A.13) of the appendix. The actual projectile system will, admittedly, be much more complex than the adopted model. However, it is reasonable to consider that a realistic description of the projectile is compatible with the model calculation where the electric dipole matrix elements have been suitably adjusted. So we are entitled to replace the model cross section σ_i^m in Eq. (7) by the measured cross section σ_i^e and then infer an "experimental" value for the $B(E1)$ distribution using:

$$B^e(E1,\varepsilon_i) = B^0(E1,\varepsilon_i)\left(1+2\frac{\sigma_i^e-\sigma_i^0}{\sigma'_i}\right). \quad (8)$$

In order to understand the relation between cross sections and $B(E1)$ values using the present method, it is useful to take a glance at Fig. 3, to be discussed in more detail in the next section, once all the elements in the calculations are introduced. In this figure each panel represents the differential cross section of the ^{11}Be+^{208}Pb reaction at a certain bombarding energy, for a particular excitation energy, versus the $B(E1)$ of ^{11}Be for the same excitation energy. Consider first the red open circle, which corresponds to the theoretical $B(E1)$ at this excitation energy and its associated computed cross section. This is to be compared with the horizontal band, that corresponds to the experimental cross section. They do not coincide, but we can now perform a series of calculations renormalizing the dipole couplings by $\delta(\varepsilon_i) = -0.4, -0.3\ldots, +0.1$, giving rise to the full circles. Note the linearity previously mentioned between cross sections and $B(E1)$. Now, if we want to extract an experimental $B(E1)$ value consistent with the experimental cross section, we just need to look at the intercept of the horizontal band, representing the experimental cross sections, with the red line, representing the family of renormalized model calculations. The extracted $B(E1)$ value is given by the red vertical dashed line.

It should be stressed that the $B(E1)$ values obtained by this procedure are unfolded from the experimental energy resolution, because the values of σ_i^0 and σ'_i are calculated integrating over the same energy and angular resolution of σ_i^e, taking into account the energy dependence of the model $B(E1)$ distribution $dB^0(E1,\varepsilon)/d\varepsilon$.

3. Application to ^{11}Be

We will apply the outlined procedure to the extraction of the $B(E1)$ distribution of ^{11}Be. We consider two experiments carried out for this purpose using the reaction ^{11}Be on ^{208}Pb. The first one is the experiment by Palit et al. [8] performed at GSI at 520 MeV/u. The other experiment was performed by Fukuda et al. [15] at RIKEN at 69 MeV/u. Both experiments measured breakup cross sections, and derived the $B(E1)$ distribution making use of the EPM, producing results that are not compatible at low breakup energies. In this context, we note that a recent *ab-initio* calculation by Calci et al. [20], based on the no-core shell model with continuum (NCSMC), predicts a $B(E1)$ distribution in good agreement with the one extracted in the RIKEN experiment [15]. However, a recent eikonal calculation performed in Ref. [21] for the GSI data, using a structure model adjusted to reproduce the main features of the *ab-initio* calculation, overestimates the energy differential cross section from this experiment at the peak.

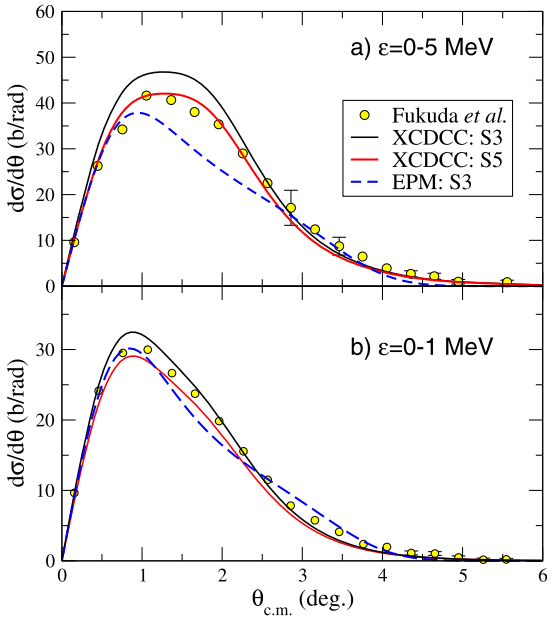

Fig. 1. Differential angular cross section for ^{11}Be+^{208}Pb breakup at 69 MeV/u for n-^{10}Be relative energies up to 5 MeV (upper panel) and up to 1 MeV (lower panel). The solid curves are XCDCC calculations with the S3 and S5 structure models, whereas the dashed line is the EPM result with model S3. All calculations have been convoluted with the experimental resolution [15].

In the present study, the ^{11}Be structure is described using a two-body (n+^{10}Be) particle-plus-rotor model (PRM) with the Hamiltonian of Ref. [22]. To account for the coupling with the 2^+ state of the ^{10}Be core, the n+^{10}Be central potential is deformed using a deformation parameter β_2 = 0.67, giving rise to core-excited admixtures in the ^{11}Be states. In Ref. [22], several sets of parameters are considered for the central and spin-orbit parts, which result in different $B(E1)$ strengths. In this work, we present results with the sets III and V of Table I of [22] which will be denoted hereafter as S3 and S5, respectively.

We have performed continuum-discretized coupled-channels calculations, including the ^{10}Be excitation (XCDCC) [16,17]. These calculations require the optical model potentials for n-^{208}Pb and ^{10}Be-^{208}Pb, with the latter including quadrupole deformation to account for possible excitations of ^{10}Be during the reaction. For the reaction at 520 MeV/u, the n-^{208}Pb potential was generated by folding the Paris-Hamburg g-matrix NN effective interaction [23,24] with the ground-state density of the target, obtained from a Hartree-Fock calculation. For the reaction at 69 MeV/u, the n-^{208}Pb potential was taken from the global parameterization of Koning and Delaroche [25]. The ^{10}Be-^{208}Pb potential consists of a double folding of the projectile and target densities with an effective g-matrix NN interaction, appropriate for each energy regime, namely, the Brùyeres Jeukenne-Lejeune-Mahaux [26,27] for the 69 MeV/u data (see also [28,29]) and the CEG07 interaction [30,31] for the 520 MeV/u data. Kinematical relativistic corrections were taken into account in both calculations, following [32]. Dynamical relativistic corrections were not included, but test calculations using the eikonal CDCC method with relativistic effects [33], gave corrections not larger than 2%-3% [34]. The calculated differential cross sections were convoluted with experimental angular and energy resolutions quoted in Refs. [8,15].

The experimental and calculated breakup angular distributions for the incident energy at 69 MeV/u are shown in Fig. 1. It can be

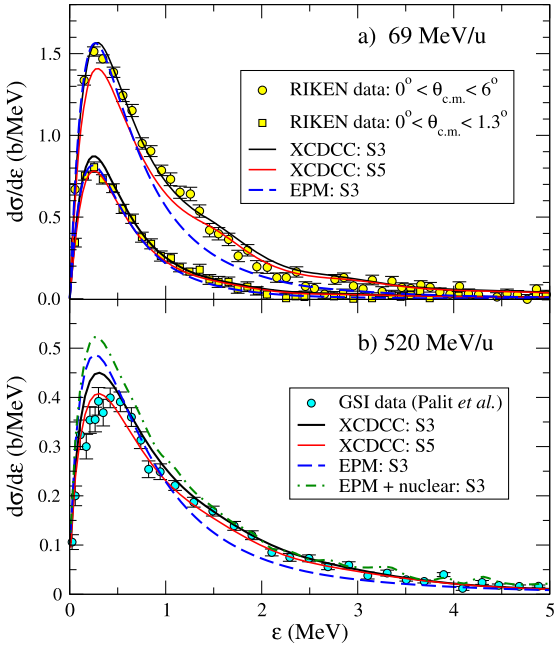

Fig. 2. Energy differential cross section for ^{11}Be+^{208}Pb breakup at 69 MeV/u (top) and 520 MeV/u (bottom). The data from Refs. [15] and [8] are compared with XCDCC calculations (solid lines) using S3 and S5 structure models and with EPM calculations (dashed lines) with S3 model. In the 520 MeV/u case, the dash-dotted line shows the result of adding the estimated nuclear breakup in Ref. [8] to the EPM result.

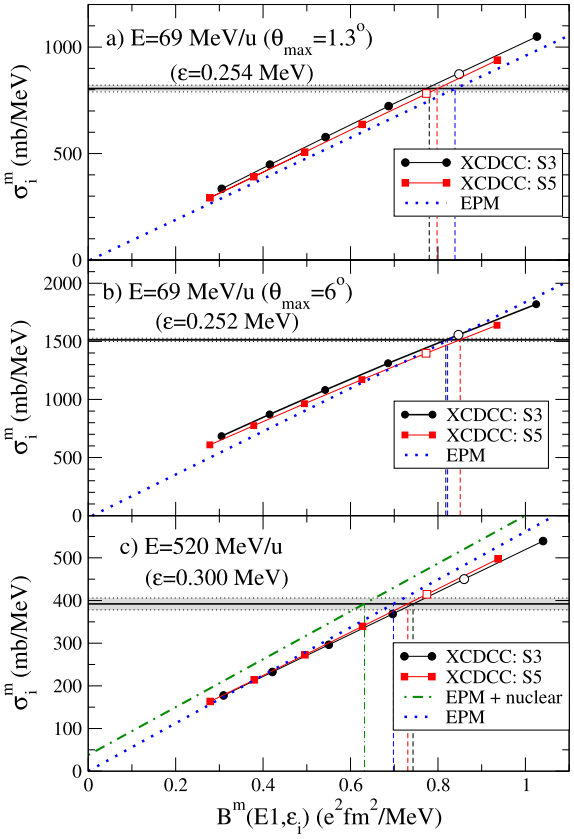

Fig. 3. Relation between the $B(E1)$ values and associated cross sections computed with XCDCC (for S3 and S5 models) and with the EPM. The shaded area in each panel corresponds to the experimental cross sections, with the corresponding uncertainty [8,15]. In the 520 MeV/u case, the dash-dotted line shows the result of adding the estimated nuclear breakup in Ref. [8] to the EPM result. The vertical lines correspond to the extracted $B(E1)$ values. The symbols correspond to model calculations for different values of δ, with the hollow ones corresponding to the $\delta = 0$ cases. See text for details.

seen that the XCDCC method gives significantly larger cross sections as compared to the EPM calculations. Moreover, the XCDCC calculation reproduces well the shape of the angular distribution, even at relatively large scattering angles, for which the nuclear interaction will be relevant. The EPM angular distributions differ significantly from the data.

Breakup energy distributions are shown in Fig. 2(a) for two angular ranges: $0° < \theta_{\rm c.m.} < 1.3°$, which is considered to be "safe Coulomb", and $0° < \theta_{\rm c.m.} < 6°$, where nuclear effects are relevant. The EPM calculation based on the $B(E1)$ distribution given by the model S3 reproduces well both sets of experimental data for breakup energies around the peak (∼0-1 MeV). However, it underestimates the cross sections at higher excitation energies (∼1-2 MeV). This could be due to limitations of the EPM dynamics, but also to limitations of the S3 structure model. To disentangle these two effects, we compare the EPM result with a XCDCC calculation based on the same S3 structure model. For the "safe Coulomb" angular range, the XCDCC cross sections are slightly larger than the EPM ones, over all the energy range. For the larger angular range, both calculations agree well at the peak, but the XCDCC calculation is significantly larger at higher excitation energies (ε ∼1-2 MeV), and agrees well with the data. Our conclusion is that there is no accurate "safe Coulomb" angular range, and that dynamical effects included in the XCDCC calculations are specially important for higher breakup energies and larger angles.

For the experiment at 520 MeV/u, no angular distribution was extracted in [8] so we focus on the angle-integrated energy differential cross section, presented in Fig. 2(b). In addition to the pure EPM calculation, we present the curve resulting from the incoherent addition of this EPM calculation with the nuclear breakup contribution estimated in Ref. [8]. As emphasized by several authors (see e.g. [35]), this procedure is clearly not justified, since it ignores Coulomb-nuclear interference. Nevertheless, we adopt it here in order to follow as closely as possible the procedure of the original analysis of these data and compare with our method, in which Coulomb-nuclear interference is properly taken into account. The resulting EPM distribution largely overestimates the data. By contrast, the XCDCC calculations, based on S3 and S5 models, have a better agreement with the data, with some overestimation of the former.

In Fig. 3 we illustrate the extraction of the $B(E1)$ from the experimental cross sections, with the method proposed in this work [Eq. (8)] and using the EPM [Eq. (4)]. In the latter (dotted lines), the relation is strictly linear, and the slope is given by the dipole Coulomb excitation function, which is model independent [cf. Eq. (1)]. For the higher incident energy, we show the EPM with and without the addition of the nuclear contribution estimated for this excitation energy. The solid lines are the XCDCC cross sections for different initial $B(E1)$ distributions, obtained by scaling the dipole couplings by $\delta(\epsilon_i)$ factors ranging from -0.4 to 0.1. It is seen that the relation between σ_i and $B(E1, \varepsilon_i)$ is linear to a very good approximation, thus supporting Eq. (7). However, the slope of the EPM line differs significantly from that of the XCDCC calculations, leading to markedly different extracted $B(E1)$ values. The slope of the XCDCC calculations, although model dependent, contains Coulomb-nuclear interference, as well as other dynamical effects which are absent in the EPM calculations. Note also that the $B(E1)$ values extracted using the EPM at the two different collision energies are significantly different, while those extracted from the XCDCC calculations are more compatible.

In Fig. 4, we compare the extracted $B(E1)$ values, using both S3 and S5 models (black and red symbols), with those obtained in the original analyses of the two considered experiments (yellow and cyan symbols). We include also the theoretical values of the S3

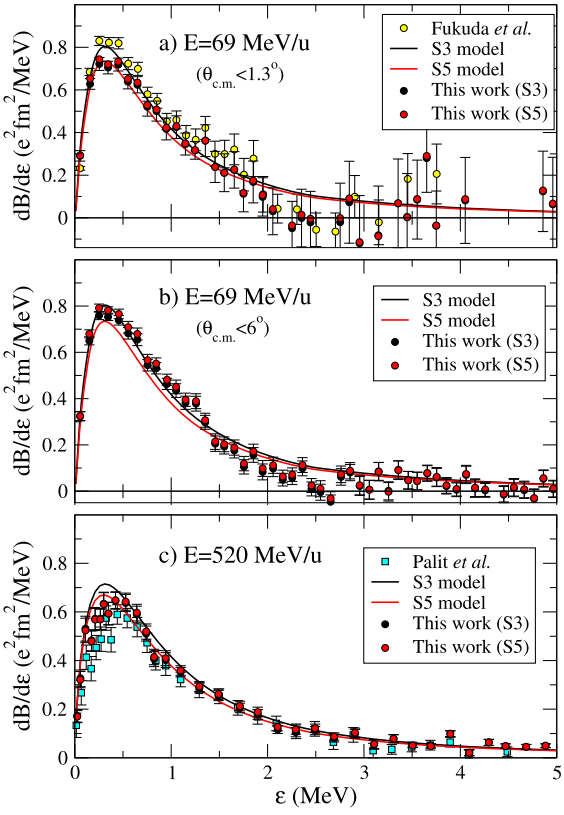

Fig. 4. $B(E1)$ distributions extracted from the ^{11}Be+^{208}Pb breakup data at 69 MeV/u and 520 MeV/u. The distributions reported in the original analyses [8,15] are compared with those extracted in the present work, starting with the structure models S3 and S5 described in the text. The latter are convoluted with the experimental energy resolution.

and S5 models (solid lines). For a meaningful comparison with the previous data, we have included in the calculations the effect of the experimental resolution quoted for each experiment. For that, we have convoluted the model $B(E1)$ distribution in Eq. (8). For the RIKEN data, we show separately the results for the angular intervals $\theta_{\rm c.m.} \leq 1.3°$ (top panel) and $\theta_{\rm c.m.} \leq 6°$ (middle panel). In the former we see that our derived $B(E1)$ agrees rather well with that from the original analysis for relative energies above 1 MeV, but is somewhat lower at the peak, due to the dynamical effects discussed previously. For the GSI data (bottom panel), our extracted $B(E1)$ agrees also very well with that of Ref. [8] but it is slightly higher at the peak. These two effects go in the direction of making the results of the two experiments more compatible. It is also noticeable that the S3 and S5 models, while predicting rather different cross sections [cf. Figs. 2 and 3], give rise to fully consistent $B(E1)$ distributions once they are corrected following the present procedure.

Note that the error bars in the extracted $B(E1)$ include the experimental uncertainty of the cross sections only. We have performed a preliminary estimation of the systematic uncertainties introduced by the model dependence (comparing S3 and S5 models), the choice of the nuclear potentials (using different prescriptions for fragment-target interactions) and non-linearity in the relation between the $B(E1)$ and the cross section. These sources of systematic uncertainties are found to be similar or smaller than the experimental uncertainties. We expect to deepen the uncertainty analysis in future publications.

To compare the $B(E1)$ extracted from the two experiments, we present unfolded $B(E1)$ values in Fig. 5. They are obtained using Eq. (8) with the model S3 $B(E1)$ distribution. For comparison, we include also the theoretical curves obtained with the original

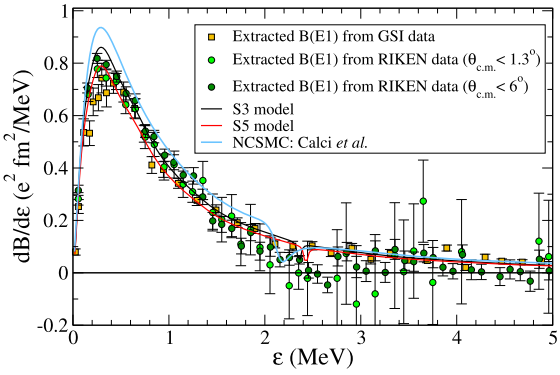

Fig. 5. Unfolded $B(E1)$ distributions extracted from the experimental breakup data from Refs. [8] (squares) and [15] (circles) using the present method starting with model S3. For comparison, the original S3 and S5 models (black and red curves) and the NCSMC *ab-initio* calculation of Ref. [20] (blue line) are also shown.

S3 and S5 models as well as the NCSMC *ab-initio* calculation by Calci et al. [20] based on the N^{2}LO$_{\rm SAT}$ interaction. For the high-energy data at 520 MeV/u, our derived values are significantly larger than those extracted in the original EPM analysis [8]. This is partly due to the effect of the energy convolution. We also present the $B(E1)$ distributions extracted from the data at 69 MeV/u for the angular ranges $\theta_{\rm c.m.} \leq 1.3°$ and $\theta_{\rm c.m.} \leq 6°$. Note the relatively larger error bars for the smaller angular range, stemming from the smaller cross sections for this interval. The $B(E1)$ extracted from the data up to 6° are indeed affected by the nuclear interaction, but these effects are explicitly considered in our procedure. Notice the remarkable agreement of the three derived distributions. Our extracted $B(E1)$ values from the two experiments turn out to be fully consistent and hence no discrepancy between the measured cross sections is apparent from our analysis. The $B(E1)$ values are consistent with the NCSMC distribution of [20] for the higher excitation energies, but are somewhat smaller at the peak. This discrepancy would deserve further investigation which goes beyond of the scope of the present work.

The present results solve the long-standing controversy between these two measurements. Furthermore, it shows that a proper description of the reaction, including Coulomb and nuclear effects on an equal footing, is necessary for a meaningful extraction of structure information of the projectile. We consider that the present procedure for extracting $B(E1)$ distributions from Coulomb-dominated breakup cross section data can be applied to other exotic nuclei, which are currently being measured at radioactive beam facilities such as RIKEN, MSU and GSI-FAIR.

Declaration of competing interest

The authors declare that they have no known competing financial interests or personal relationships that could have appeared to influence the work reported in this paper.

Acknowledgements

We are grateful to Takashi Nakamura and Thomas Aumann for discussions on the RIKEN and GSI data analysed in this work, to Kazuyuki Ogata for useful feedback on the relativistic corrections and to T. Furumoto and D. Pang for providing us the double-folding g-matrix potentials employed in our calculations. This work has been partially supported by the Spanish Ministerio de Ciencia, Innovación y Universidades and FEDER funds under projects FIS2017-88410-P and RTI2018-098117-B-C21 and by the European Union's Horizon 2020 research and innovation program under Grant Agreement No. 654002.

Appendix A. Amplitude analysis

In this appendix we justify the use of a correction factor determined from the differential cross sections, to obtain the experimental $B(E1)$ distribution.

Consider a model calculation, involving some nuclear and Coulomb couplings, which are considered to all orders. A general quantum mechanical treatment of Coulomb dissociation experiments leads to cross sections which are given by an integral over the angular range and the energy resolution of the calculated double differential cross section

$$\sigma_i^0 = \int dx\, R(\varepsilon_i, x) \frac{d^2\sigma^0}{d\Omega d\varepsilon}, \tag{A.1}$$

where $R(\varepsilon_i, x)$ represents the experimental angular and energy resolutions and $x = (\Omega, \varepsilon)$ incorporates both the centre of mass angle and the energy of the break-up fragments. The double differential cross section contains, in turn, an average over the ground state spin projection N, as well as a sum over the break-up states M compatible with the energy ε, of the square of the transition amplitudes connecting them. The discrete index M labels completely the break-up states, so it includes the core angular momentum, the halo neutron orbital angular momentum, the halo neutron total angular momentum, the total angular momentum of the halo nucleus, and its spin projection:

$$\frac{d^2\sigma^0}{d\Omega d\varepsilon} = \overline{\sum_{NM}} |A(N, M, x)|^2 \tag{A.2}$$

where $\overline{\sum}_{NM}$ indicates this sum over final states M and average over the initial states N. In Coulomb dominated breakup reactions, the amplitude $A(N, M, x)$, is dominated by a dipole Coulomb term which is proportional to the Coulomb dipole matrix element, so that $A_C(N, M, x) = \langle N|\mathcal{M}(E1)|M, \varepsilon\rangle A_D(x)$, but it will also have an extra term $A_n(N, M, x)$, containing the nuclear component, as well as other higher order Coulomb components, which we do not want to neglect. Note that we do not have to make any assumption about the specific expression $A_D(x)$. In particular, we do not need to make any semi-classical assumption, nor do we have to neglect the effect of nuclear forces or other dynamical effects. We only assume that the general amplitude $A(N, M, x)$ has a dependence on the initial and final states N, M, which has a dominant term proportional to $\langle N|\mathcal{M}(E1)|M, \varepsilon\rangle$, and an additional, smaller term $A_n(N, M, x)$, with a different N, M dependence. The model will produce a $B(E1)$ distribution

$$\frac{dB^0(E1, \varepsilon)}{d\varepsilon} = \overline{\sum_{NM}} |\langle N|\mathcal{M}(E1)|M, \varepsilon\rangle|^2, \tag{A.3}$$

which, particularized at the experimental energies, becomes

$$B^0(E1, \varepsilon_i) = \overline{\sum_{NM}} |\langle N|\mathcal{M}(E1)|M, \varepsilon_i\rangle|^2, \tag{A.4}$$

and the associated differential cross sections

$$\frac{d^2\sigma^0}{d\Omega d\varepsilon} = \overline{\sum_{MN}} |\langle N|\mathcal{M}(E1)|M, \varepsilon\rangle A_D(x) + A_n(N, M, x)|^2. \tag{A.5}$$

Expression (A.5) indicates that the measured cross section is not proportional to the $B(E1)$ distribution, as assumed in the EPM. It also indicates that, owing to the presence of interference terms, it is not possible to estimate the nuclear effects as a nuclear cross section to be added to the pure Coulomb one. In spite of that, we will see how it is possible to obtain the $B(E1)$ distribution from these cross sections.

Consider now that we make arbitrary small changes in the model. This will result in small changes in all the Coulomb dipole couplings, in particular, those connecting the ground state with the continuum states, that can be described by factors $(1+\delta(N, M, \varepsilon))$, where $\delta(N, M, \varepsilon)$ are arbitrary small numbers. The nuclear couplings could in principle be also modified, producing small changes in $A_n(N, M, x)$. However, as the nuclear amplitudes are already small compared to the Coulomb ones, their small changes would be a second order effect, that can be neglected. For this modified model, the $B(E1)$ distribution is approximately given by

$$\frac{dB^m(E1, \varepsilon)}{d\varepsilon} \simeq \overline{\sum_{MN}} (1 + 2\delta(N, M, \varepsilon)) |\langle N|\mathcal{M}(E1)|M, \varepsilon\rangle|^2 = (1 + 2\delta(\varepsilon)) \frac{dB^0(E1, \varepsilon)}{d\varepsilon}, \tag{A.6}$$

where $\delta(\varepsilon)$ is a weighted average of the $\delta(NM, \varepsilon)$ values corresponding to the different dipole couplings between the ground state and the states with energy ε, i.e.,

$$\delta(\varepsilon) = \frac{\overline{\sum}_{NM} \delta(N, M, \varepsilon) |\langle N|\mathcal{M}(E1)|M, \varepsilon\rangle|^2}{\overline{\sum}_{NM} |\langle N|\mathcal{M}(E1)|M, \varepsilon\rangle|^2}. \tag{A.7}$$

This expression can be particularized at the experimental energies ε_i, leading to

$$B^m(E1, \varepsilon_i) \simeq (1 + 2\delta(\varepsilon_i)) B^0(E1, \varepsilon_i). \tag{A.8}$$

Let us now consider the effect on the cross sections. The modified differential cross sections are

$$\sigma_i^m = \int dx R(\varepsilon_i, x) \overline{\sum_{MN}} |(1 + \delta(N, M, \varepsilon)) A_C(N, M, x) + A_n(N, M, x)|^2. \tag{A.9}$$

This can be expanded to the lowest order in the small parameters $\delta(N, M, \varepsilon)$. Also, considering that the energy range for $R(\varepsilon_i, x)$ is sufficiently narrow, compared to the energy dependence of the electric matrix elements, one can take $\delta(N, M, \varepsilon)$ and $\langle N|\mathcal{M}(E1)|M, \varepsilon\rangle$ out of the integral, and evaluate them at the nominal energy ε_i. Note, however, that we do not need to make any assumption about the energy dependence of the amplitude $A_D(x)$.

$$\sigma_i^m \simeq \sigma_i^0 + \overline{\sum_{MN}} \delta(N, M, \varepsilon_i) |\langle N|\mathcal{M}(E1)|M, \varepsilon_i\rangle|^2 \times \int dx R(\varepsilon_i, x) \left(2|A_D(x)|^2 + \frac{A_D(x) A_n^*(N, M, X)}{\langle N|\mathcal{M}(E1)|M, \varepsilon_i\rangle^*} + cc \right). \tag{A.10}$$

In a Coulomb-dominated reaction, the dipole amplitude $|A_D(x)|^2$ dominates over the Coulomb-nuclear interference term, and hence the term in parentheses is approximately independent of the final dipole state. This justifies replacing $\delta(N, M, \varepsilon_i)$ by the weighted average $\delta(\varepsilon_i)$ given by Eq. (A.7). It also justifies neglecting any small correction of the nuclear amplitudes. Thus we get

$$\sigma_i^m \simeq \sigma_i^0 + \delta(\varepsilon_i) \sigma_i', \tag{A.11}$$

where

$$\sigma_i' = \overline{\sum_{MN}} |\langle N|\mathcal{M}(E1)|M, \varepsilon_i\rangle|^2 \times \int dx\, R(\varepsilon_i, x) \left(2|A_D(x)|^2 + \frac{A_D(x) A_n^*(N, M, x)}{\langle N|\mathcal{M}(E1)|M, \varepsilon_i\rangle^*} + cc \right). \tag{A.12}$$

The practical calculation of σ_i' can be done evaluating the cross sections $\sigma_i(\delta)$ at the experimental energies ε_i from model calculations where all the dipole couplings have been renormalized by factors $(1+\delta)$, using small values of δ, such as $\delta = \pm 0.1$.

$$\sigma_i' = \frac{1}{0.2}\left[\sigma_i(\delta = 0.1) - \sigma_i(\delta = -0.1)\right]. \tag{A.13}$$

References

[1] K. Alder, A. Winther, Electromagnetic Excitation: Theory of Coulomb Excitation with Heavy Ions, North-Holland Pub. Co., 1975.

[2] C.A. Bertulani, G. Baur, Electromagnetic processes in relativistic heavy ion collisions, Phys. Rep. 163 (1988) 299, https://doi.org/10.1016/0370-1573(88)90142-1.

[3] T. Glasmacher, Coulomb excitation at intermediate energies, Annu. Rev. Nucl. Part. Sci. 48 (1998) 1, https://doi.org/10.1146/annurev.nucl.48.1.1.

[4] A. Gade, D. Bazin, C.M. Campbell, J.A. Church, D.C. Dinca, J. Enders, T. Glasmacher, Z. Hu, K.W. Kemper, W.F. Mueller, H. Olliver, B.C. Perry, L.A. Riley, B.T. Roeder, B.M. Sherrill, J.R. Terry, Detailed experimental study on intermediate-energy Coulomb excitation of ^{46}Ar, Phys. Rev. C 68 (2003) 014302, https://doi.org/10.1103/PhysRevC.68.014302.

[5] H. Esbensen, G. Bertsch, C. Bertulani, Higher-order dynamical effects in Coulomb dissociation, Nucl. Phys. A 581 (1995) 107, https://doi.org/10.1016/0375-9474(94)00423-K.

[6] H. Esbensen, G.F. Bertsch, Higher-order effects in the two-body breakup of ^{17}F, Nucl. Phys. A 706 (2002) 383, https://doi.org/10.1016/S0375-9474(02)00869-2.

[7] V. Pesudo, et al., Scattering of the halo nucleus ^{11}Be on ^{197}Au at energies around the Coulomb barrier, Phys. Rev. Lett. 118 (2017) 152502, https://doi.org/10.1103/PhysRevLett.118.152502.

[8] R. Palit, et al., Exclusive measurement of breakup reactions with the one-neutron halo nucleus ^{11}Be, Phys. Rev. C 68 (2003) 034318, https://doi.org/10.1103/PhysRevC.68.034318.

[9] H. Esbensen, Coulomb dissociation of ^{15}C and radiative neutron capture on ^{14}C, Phys. Rev. C 80 (2009) 024608, https://doi.org/10.1103/PhysRevC.80.024608.

[10] N.C. Summers, F.M. Nunes, Extracting (n,γ) direct capture cross sections from Coulomb dissociation: application to ^{14}C$(n,\gamma)^{15}$C, Phys. Rev. C 78 (2008) 011601, https://doi.org/10.1103/PhysRevC.78.011601.

[11] J. Singh, T. Matsumoto, K. Ogata, Systematic study on the role of various higher-order processes in the breakup of weakly-bound projectiles, arXiv:2005.05605, 2020.

[12] D. Baye, P. Capel, G. Goldstein, Collisions of halo nuclei within a dynamical Eikonal approximation, Phys. Rev. Lett. 95 (2005) 082502, https://doi.org/10.1103/PhysRevLett.95.082502.

[13] G. Goldstein, D. Baye, P. Capel, Dynamical Eikonal approximation in breakup reactions of ^{11}Be, Phys. Rev. C 73 (2006) 024602, https://doi.org/10.1103/PhysRevC.73.024602.

[14] D. Baye, P. Capel, Breakup reaction models for two- and three-cluster projectiles, in: C. Beck (Ed.), Clusters in Nuclei, vol. 2, in: Lecture Notes in Physics, vol. 848, Springer, Berlin, Heidelberg, 2012.

[15] N. Fukuda, et al., Coulomb and nuclear breakup of a halo nucleus ^{11}Be, Phys. Rev. C 70 (2004) 054606, https://doi.org/10.1103/PhysRevC.70.054606.

[16] N.C. Summers, F.M. Nunes, I.J. Thompson, Extended continuum discretized coupled channels method: core excitation in the breakup of exotic nuclei, Phys. Rev. C 74 (2006) 014606, https://doi.org/10.1103/PhysRevC.74.014606.

[17] R. de Diego, J.M. Arias, J.A. Lay, A.M. Moro, Continuum-discretized coupled-channels calculations with core excitation, Phys. Rev. C 89 (2014) 064609, https://doi.org/10.1103/PhysRevC.89.064609.

[18] J.A. Lay, A.M. Moro, J.M. Arias, J. Gomez-Camacho, Exploring continuum structures with a pseudo-state basis, Phys. Rev. C 82 (2010) 024605.

[19] J.A. Lay, A.M. Moro, J.M. Arias, J. Gómez-Camacho, Particle motion in a deformed potential using a transformed oscillator basis, Phys. Rev. C 85 (2012) 054618, https://doi.org/10.1103/PhysRevC.85.054618.

[20] A. Calci, P. Navrátil, R. Roth, J. Dohet-Eraly, S. Quaglioni, G. Hupin, Can ab initio theory explain the phenomenon of parity inversion in ^{11}Be?, Phys. Rev. Lett. 117 (2016) 242501, https://doi.org/10.1103/PhysRevLett.117.242501.

[21] L. Moschini, P. Capel, Reliable extraction of the $dB(E1)/dE$ for ^{11}Be from its breakup at 520 MeV/nucleon, Phys. Lett. B 790 (2019) 367, https://doi.org/10.1016/j.physletb.2019.01.041.

[22] N. Summers, S. Pain, N. Orr, W. Catford, J. Angélique, N. Ashwood, V. Bouchat, N. Clarke, N. Curtis, M. Freer, B. Fulton, F. Hanappe, M. Labiche, J. Lecouey, R. Lemmon, D. Mahboub, A. Ninane, G. Normand, F. Nunes, N. Soić, L. Stuttge, C. Timis, I. Thompson, J. Winfield, V. Ziman, $B(E1)$ strengths from Coulomb excitation of ^{11}Be, Phys. Lett. B 650 (2007) 124, https://doi.org/10.1016/j.physletb.2007.05.003.

[23] H.V. von Geramb, Microscopic optical potentials, AIP Conf. Proc. 97 (1983) 44, https://doi.org/10.1063/1.33973.

[24] L. Rikus, K. Nakano, H.V. Von Geramb, Microscopic analysis of elastic and inelastic proton scattering from ^{12}C, Nucl. Phys. A 414 (1984) 413, https://doi.org/10.1016/0375-9474(84)90611-0.

[25] A. Koning, J. Delaroche, Local and global nucleon optical models from 1 keV to 200 MeV, Nucl. Phys. A 713 (2003) 231, https://doi.org/10.1016/S0375-9474(02)01321-0.

[26] E. Bauge, J.P. Delaroche, M. Girod, Semimicroscopic nucleon-nucleus spherical optical model for nuclei with $A > \sim 40$ at energies up to 200 MeV, Phys. Rev. C 58 (1998) 1118, https://doi.org/10.1103/PhysRevC.58.1118.

[27] E. Bauge, J.P. Delaroche, M. Girod, Lane-consistent, semimicroscopic nucleon-nucleus optical model, Phys. Rev. C 63 (2001) 024607, https://doi.org/10.1103/PhysRevC.63.024607.

[28] D.Y. Pang, private communication.

[29] Y.P. Xu, D.Y. Pang, Toward a systematic nucleus-nucleus potential for peripheral collisions, Phys. Rev. C 87 (2013) 044605, https://doi.org/10.1103/PhysRevC.87.044605.

[30] T. Furumoto, private communication.

[31] T. Furumoto, W. Horiuchi, M. Takashina, Y. Yamamoto, Y. Sakuragi, Global optical potential for nucleus-nucleus systems from 50 MeV/u to 400 MeV/u, Phys. Rev. C 85 (2012) 044607, https://doi.org/10.1103/PhysRevC.85.044607.

[32] A.M. Moro, Three-body model for the analysis of quasifree scattering reactions in inverse kinematics, Phys. Rev. C 92 (2015) 044605, https://doi.org/10.1103/PhysRevC.92.044605.

[33] K. Ogata, C.A. Bertulani, Dissociation of relativistic projectiles with the continuum-discretized coupled-channels method, Prog. Theor. Phys. (Kyoto) 121 (2009) 1399, https://doi.org/10.1143/PTP.121.1399.

[34] K. Ogata, private communication.

[35] M. Hussein, R. Lichtenthäler, F. Nunes, I. Thompson, Scaling and interference in the dissociation of halo nuclei, Phys. Lett. B 640 (2006) 91, https://doi.org/10.1016/j.physletb.2006.07.046.